applied sciences

MDPI

Article

Ni_3Se_4@$MoSe_2$ Composites for Hydrogen Evolution Reaction

Wenwu Guo [1,†], Quyet Van Le [2,†], Ha Huu Do [1], Amirhossein Hasani [1], Mahider Tekalgne [1], Sa-Rang Bae [1], Tae Hyung Lee [3], Ho Won Jang [3,*], Sang Hyun Ahn [1,*] and Soo Young Kim [4,*]

1 School of Chemical Engineering and Materials Science, Chung-Ang University, Seoul 06974, Korea; guowenwu95@gmail.com (W.G.); hadohuu1311@gmail.com (H.H.D.); amirhossein.hasani88@gmail.com (A.H.); maddy.missy@gmail.com (M.T.); dngorl147@naver.com (S.-R.B.)
2 Institute of Research and Development, Duy Tan University, Da Nang 550000, Vietnam; quyetbk88@gmail.com
3 Department of Materials Science and Engineering, Research Institute of Advanced Materials, Seoul National University, Seoul 08826, Korea; sunshinety@snu.ac.kr
4 Department of Materials Science and Engineering, Korea University 145, Anam-ro Seongbuk-gu, Seoul 02841, Korea
* Correspondence: hwjang@snu.ac.kr (H.W.J.); shahn@cau.ac.kr (S.H.A.); sooyoungkim@korea.ac.kr (S.Y.K.)
† Wenwu Guo and Quyet Van Le contributed equally to this work.

Received: 5 November 2019; Accepted: 20 November 2019; Published: 22 November 2019

Featured Application: The Ni_3Se_4@$MoSe_2$ composites could be used as electrocatalyst for hydrogen production.

Abstract: Transition metal dichalcogenides (TMDs) have been considered as one of the most promising electrocatalysts for the hydrogen evolution reaction (HER). Many studies have demonstrated the feasibility of significant HER performance improvement of TMDs by constructing composite materials with Ni-based compounds. In this work, we prepared Ni_3Se_4@$MoSe_2$ composites as electrocatalysts for the HER by growing in situ $MoSe_2$ on the surface of Ni_3Se_4 nanosheets. Electrochemical measurements revealed that Ni_3Se_4@$MoSe_2$ nanohybrids are highly active and durable during the HER process, which exhibits a low onset overpotential (145 mV) and Tafel slope (65 mV/dec), resulting in enhanced HER performance compared to pristine $MoSe_2$ nanosheets. The enhanced HER catalytic activity is ascribed to the high surface area of Ni_3Se_4 nanosheets, which can both efficiently prevent the agglomeration issue of $MoSe_2$ nanosheets and create more catalytic edge sites, hence accelerate electron transfer between $MoSe_2$ and the working electrode in the HER. This approach provides an effective pathway for catalytic enhancement of MoSe2 electrocatalysts and can be applied for other TMD electrocatalysts.

Keywords: hydrogen evolution reaction; $MoSe_2$; Ni_3Se_4; nanoflowers; nanosheets

1. Introduction

Energy-saving and environmental protection are of great importance to develop a sustainable society in the 21st century. Currently, 80% of global energy is produced by the consumption of fossil fuels. However, the unsustainable fossil fuels will ultimately come to depletion because of the continuously growing population and expanding industrialization in the world, and their consumption will also lead to serious environmental pollution. So, there is an urgent need to explore alternative energy resources to substitute fossil fuels and gradually switch to a society dominated by sustainable and renewable energy [1,2]. Hydrogen energy is considered as one of the promising clean and renewable energies [3–7] because it possesses high energy density and its only outcome by combustion

is water. These properties make it a highly efficient and environmentally friendly energy and enable its potential to replace the current traditional fossil fuels. Its production from electrolytic water is an important key to realize industrialization because this path for conversion of electricity to chemical energy has many advantages, such as low cost, being friendly to the environment, high efficiency, and good safety [8–10]. To achieve the best efficiency, this conversion process largely demands the assistance of a highly active hydrogen evolution reaction (HER) electrocatalyst [10,11]. To date, platinum is considered as the most efficient catalyst for hydrogen evolution [12–15]. However, its scarcity on earth and high price make it unsuitable for widespread adoption. A few recent works have demonstrated high catalytic activity using less Pt on electrodes [16]. Nevertheless, it is still necessary to explore earth-abundant and inexpensive electrocatalysts for hydrogen production [17–20].

Among the catalyst candidates, layered transitional metal dichalcogenides MX, where M represents a transition metal (e.g., Mo, W, V) and X is a chalcogenide (e.g., S, Se, Te), have drawn great attention due to their attractive electrocatalytic properties towards HER, as well as their low cost compared to noble metals and stability in acid [21–24]. However, only the edges, rather than the basal planes within the material structure, are catalytically active to HER [23,25–28]. In order to expose more active edges, intense efforts have been made on active edge engineering by hybridizing with other materials, such as carbon nanotubes, graphene, and noble metals, to improve their conductivity and accelerate the electron transfer rate between the electrocatalyst and the working electrode [11,29–31]. Recently, some studies have reported that Ni-based materials, such as NiSe nanofiber [32–34], Ni–Mo alloy [35–37], and transition metal dichalcogenides (TMDs) integrated with Ni components [5,37,38], exhibited great catalytic activity and long-term stability for water splitting. Inspired by this viewpoint, we consciously chose one of the selenides of nickel as a candidate for structuring Ni-based components/$MoSe_2$ hybrid composites for hydrogen production. Among all nickel selenides, Ni_3Se_2 has been intensively studied and hybrid materials based on them have been extensively reported [39–41]. However, the common methods employed to obtain nickel selenides, such as hydrothermal technique or electrodeposition, are either time-consuming or energy-consuming processes. Therefore, it is imperative to use a facile preparation method for these compounds and facilitate their integration with other materials and make it applicable to large-scale HER catalysts.

In this study, we presented a $Ni_3Se_4/MoSe_2$ composites catalyst fabricated by a facial two-step synthesis method for the first time. The Ni_3Se_4 was prepared in a simple way as a template and the $MoSe_2$ was grown in situ on as-prepared Ni_3Se_4 using the colloid synthesis method. The Ni_3Se_4 nanosheets are expected to support the nucleation and formation of $MoSe_2$, which can improve the quality of the $MoSe_2$ nanosheets and prevent the agglomeration issue associated with Ni_3Se_4 and $MoSe_2$. The simplification of preparing Ni_3Se_4 makes it easier to tune and control the proportion of the components in $Ni_3Se_4/MoSe_2$ composites. The HER test results showed that the Ni_3Se_4@$MoSe_2$ catalysts exhibited improved HER activity with low onset overpotential (140 mV) and Tafel slope (67 mV/dec) compared to pure $MoSe_2$ nanosheets (80 mV/dec). The high catalytic activity of the $Ni_3Se_4/MoSe_2$ composites with a simple way of fabrication makes it competitive to other Ni-based $MoSe_2$ electrocatalysts in practical application.

2. Experimental Section

2.1. Materials

Nickel (II) chloride hexahydrate [$NiCl_2{\cdot}6H_2O$, 98%], molybdenum hexacarbonyl (Mo $(CO)_6$), selenium (99.999%), 1-octadecene (ODE, 90%, tech), 1-dodecanethiol, and acetic acid were purchased from Sigma-Aldrich. Oleylamine (OAm, 80–90%) was purchased from Acros Organics. All reagents were analytical grade and used as received without further purification.

2.2. Synthesis of Ni_3Se_4 Nanosheets

Ni_3Se_4 nanoparticles were synthesized as in previous work with some modifications [42]. In a typical synthesis procedure, 0.1 M NaOH solutions were prepared by dissolving 0.1 mol NaOH in 100 mL of ethanol. Subsequently, 12 mL of the solution was taken in each spout of a three-neck flask. Then, 0.2 mM $NiCl_2 \bullet 6H_2O$, 0.2 mM selenium powder, and 2 mL of $N_2H_4 \bullet H_2O$ were added to the bottles, which were sealed well and preserved at 90 °C for 16 h with magnetic stirring. Thereafter, the black powders were collected by centrifugation and washed with ethanol repeatedly, followed by final drying in a vacuum oven for further characterization and synthesis of composites. The final Ni_3Se_4 product weighed 98.4 mg.

2.3. Synthesis of Ni_3Se_4–$MoSe_2$ Composites

In a typical procedure, 0.2 mmol Se powder dissolved in 10 mL of OAm and dodecanethiol (9:1, vol%) was placed in a three-neck flask at room temperature. The suspension was first maintained at 120 °C for around 10 min with moderate stirring. To obtain the highly active Se precursor, the mixture was then heated up to 200 °C and aged for an additional 0.5 h. After it cooled down to room temperature, as-obtained Ni_3Se_4 nanosheets (0.05, 0.1, and 0.2 mmol) mixed with 0.1 mmol of $Mo(CO)_6$ were added into 5 mL OAm and 15 mL ODE and then sufficiently mixed before injecting into the flask (the ratios of Ni_3Se_4 to $MoSe_2$ were fixed at 1:2, 1:1, and 2:1, respectively). The products were then held at 250 °C for 0.5 h before being cooled to room temperature. Subsequently, the black powders were thoroughly washed alternately by hexane and ethanol and separated from solution by centrifugation. Further, an acid-picking process was applied to remove the organic molecules and improve the hydrophilic property of the products by dissolving them in acetic acid and maintaining them at 85 °C with vigorous magnetic stirring for 12 h. The final products were washed with alcohol, centrifuged, and dried for further characterization. Pristine $MoSe_2$ nanosheets were synthesized under the same conditions except adding Ni_3Se_4 nanosheets. The Ni_3Se_4–$MoSe_2$ composites with ratios of 1:2, 1:1, and 2:1 weighed 31.2, 52.4, and 96.8 mg, and are denoted as Sample 1, 2, and 3 in the following discussion, respectively

2.4. Characterization

X-ray powder diffraction (XRD, Bruker New D8-Advance) patterns were recorded on an X-ray powder diffractometer with CuKα radiation (λ = 0.154 nm). Field-emission scanning electron microscopy (FE-SEM, Zeiss 300 VP) images were captured at an acceleration voltage of 10 kV. Transmission electron microscopy (TEM) and energy-dispersive X-ray spectroscopy (EDX) mapping were performed using a JEOL (Tokyo, Japan) instrument. X-ray photoelectron spectroscopy (XPS) was conducted using a K-alpha plus (Thermo Fisher) instrument under vacuum pressure of at least 1×10^{-5} bar using MgKα radiation (1250 eV) and a constant pass energy of 50 eV.

2.5. Electrochemical

Characterization HER performance test was implemented using a three-electrode cell, which consisted of a glassy carbon as working electrode (GCE, 3 mm in diameter), a graphite rod as counter electrode, and a saturated calomel as reference electrode and in 0.5 M H_2SO_4 at room temperature. Then, 4 mg catalyst and 30 µL Nafion solution (5 wt%) were dispersed in 1.0 mL N, N-Dimethylformamide (DMF) and then sonicated for 0.5 h to form a homogeneous ink. Subsequently, 5 µL catalyst ink was then dropped onto the GCE and dried naturally. Linear sweep voltammetry (LSV) was performed between 0.2 and −1.0 V vs. RHE at a sweep rate of 5 mV/s. Electrochemical impedance spectroscopy (EIS) measurements were carried out in the frequency range of 10^5 to 10^{-1} Hz at the voltage of 0.27 V vs. RHE. All the potentials were calibrated to RHE using the equation: E(RHE) = E(SCE) + 0.272 mV.

3. Results and Discussion

3.1. Synthesis and Structural Characterization

Ni_3Se_4 powders were synthesized by a facile and low-temperature method in ethanol (solvent), and the composites were obtained by growing $MoSe_2$ on the as-synthesized Ni_3Se_4 nanosheets as depicted in Figure 1. The structural properties of Ni_3Se_4 and Ni_3Se_4–$MoSe_2$ powders were investigated by XRD. As displayed in Figure 2, three dominant peaks appeared at 33.1°, 44.8°, and 50.6° in the spectra of Ni_3Se_4, which were assigned to the (312), (514), and (310) crystal faces of the Ni_3Se_4 phase, respectively (PDF card number 18-0890) [43]. Further, the obtained diffraction peaks of $MoSe_2$ can be indexed to the hexagonal 2H-$MoSe_2$ (JCPDS 29-0914). The XRD patterns of Ni_3Se_4–$MoSe_2$ were like that of Ni_3Se_4, but (002) peak assigned to the basal plane of $MoSe_2$ could still be observed in the patterns.

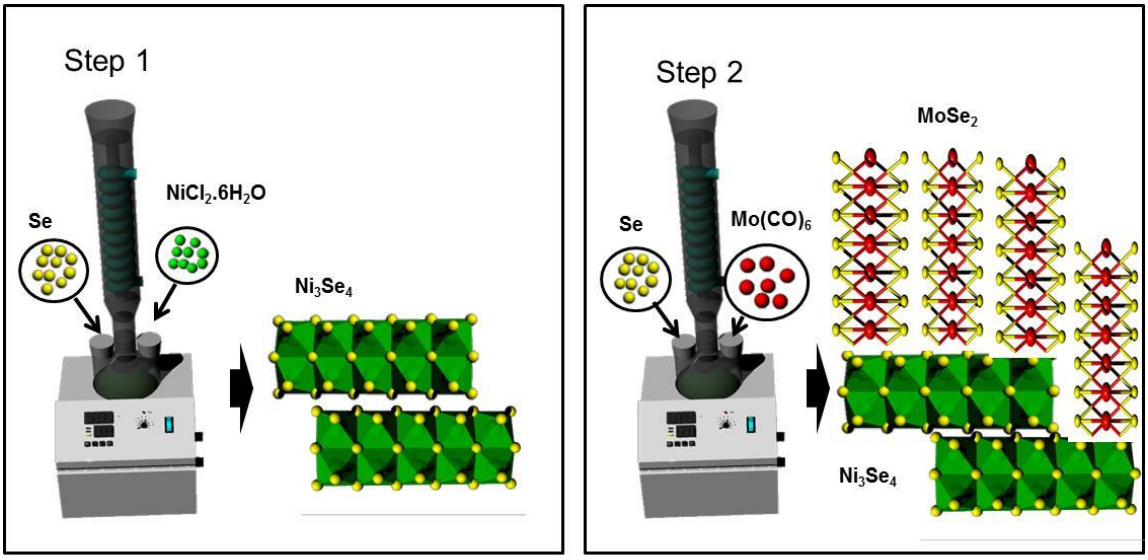

Figure 1. Synthesis of Ni_3Se_4@$MoSe_2$ composites.

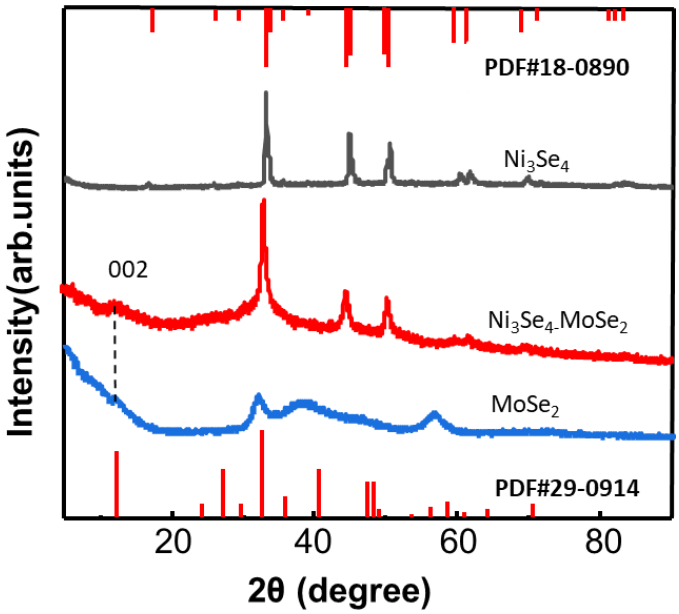

Figure 2. XRD patterns of Ni_3Se_4, Ni_3Se_4@$MoSe_2$, and $MoSe_2$.

Further, XPS analysis was carried out to explore the composition and chemical state of the composites. The survey spectrum of the Ni_3Se_4–$MoSe_2$ composites clearly shows the peaks of Ni 2p, Mo 3d, Se 3d, and O 1s (Figure 3a). The O 1s peak occurred owing to the unavoidable oxidation that takes place during the synthesis process. To confirm the oxidation states of these three elements in the composites, the high-resolution spectra of Ni 2p, Mo 3d, and Se 3d were also obtained (Figure 3b). The spectrum of Ni 2p in the Ni_3Se_4–$MoSe_2$ composites could be deconvoluted into two doublets ($2p_{3/2}$ and $2p_{1/2}$) along with two shake-up satellites, which appeared due to the spin–orbit coupling effect [44]. Specifically, the $2p_{3/2}$ peak could be further deconvoluted into two components, which were located at the band energies of 853.6 and 855.8 eV. The lower energy band could be attributed to the +2 valence state of nickel (Ni^{2+}), whereas the higher energy could be attributed to the +3 valence state of nickel (Ni^{3+}) [43,45,46]. Similarly, the $2p_{1/2}$ peak could also be resolved into two components that were located at the band energies of 870.9 and 873.5 eV, which were assigned to Ni^{2+} and Ni^{3+}, respectively [43,45,46]. Further, the satellite peaks appeared at a binding energy slightly positive to the peaks of Ni $2p_{3/2}$ and Ni $2p_{1/2}$ [45]. Compared to the spectrum of Ni 2p in pure Ni_3Se_4, all components and satellite peaks shifted slightly (approximately 0.1–1.2 eV) towards lower binding energy, which indicated the chemical bonding between Ni_3Se_4 and $MoSe_2$. For the spectra of Mo 3d (Figure 3c), the two peaks at binding energies of 229.0 and 232.2 eV were assigned to Mo $3d_{5/2}$ and Mo $3d_{3/2}$ of Mo (IV), confirming the presence of Mo^{4+}, while the peak at binding energies of 235.6 eV was probably due to the Mo oxide [47], which was formed by oxidation of the metal Mo during the synthesis process. In addition, the Se 3d spectra of the Ni_3Se_4–$MoSe_2$ composites is shown in Figure 3d. The peaks at binding energies of 54.3 and 55.2 eV were corresponded to Se $3d_{5/2}$ and Se $3d_{3/2}$, respectively, confirming the presence of Se in –2 valence state, whereas the peak at binding energies of 59.9 eV oxidized Se species (SeO_x). Further, the peaks of both Se $3d_{5/2}$ and $3d_{3/2}$ in the composites shifted slightly towards a higher binding energy, whereas the position of the SeO_x peak remained unchanged.

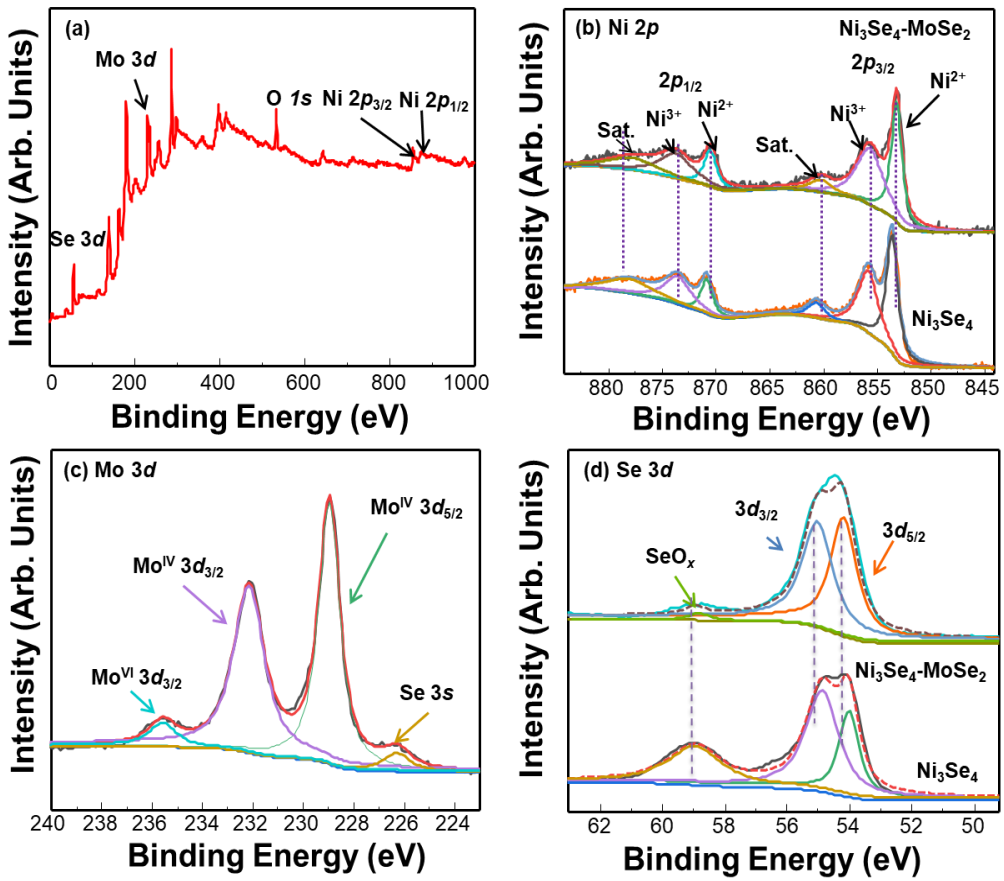

Figure 3. XPS profiles (**a**) survey, (**b**) Ni 2p, (**c**) Mo 3d, and (**d**) Se 3d.

The morphologies and structures of the Ni_3Se_4 and Ni_3Se_4–$MoSe_2$ composites with different amounts of Ni_3Se_4 were characterized by FE-SEM and TEM. Figure 4 shows the FE-SEM and TEM images of pure Ni_3Se_4 and Ni_3Se_4–$MoSe_2$ composites with a ratio of 1:2. The pure Ni_3Se_4 nanosheets were observed to be aggregated and formed clusters with large surface areas, as shown in Figure 4a. Figure 4b shows the high-resolution transmission electron microscopy (HRTEM) image of Ni_3Se_4 nanosheets with a lattice fringe of 0.27 nm, which was assigned to the (112) plane [48]. By in situ synthesis, uniform flower-like $MoSe_2$ nanosheets could be grown on Ni_3Se_4 nanosheets (Figure 4c). The growth of vertical $MoSe_2$ nanoflowers was further confirmed by HRTEM (Figure 4d). Moreover, the EDX elemental mapping results shown (Supporting Information, Figure S1) revealed that $MoSe_2$ nanoflowers were dispersed uniformly on the surface of Ni_3Se_4. Further increasing the amound of Ni_3Se_4 in the Ni_3Se_4-$MoSe_2$ composites resulted in agglomeration of the composites (Supporting Information, Figure S2) and could hinder the exposure of active edges of $MoSe_2$.

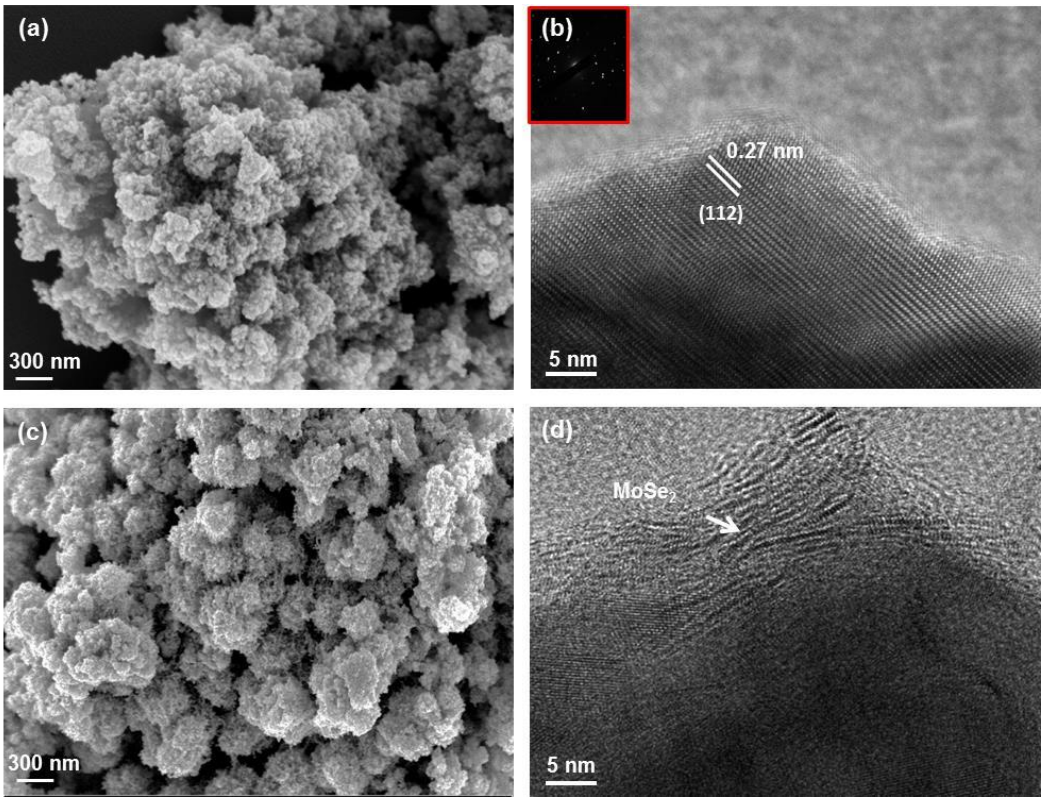

Figure 4. (**a**) FE-SEM image of Ni_3Se_4, (**b**) HRTEM image of Ni_3Se_4, (**c**) FE-SEM image of Ni_3Se_4@$MoSe_2$, and (**d**) HRTEM image of Ni_3Se_4@$MoSe_2$.

3.2. Electrocatalytic Properties

The electrocatalytic HER activities of Ni_3Se_4, $MoSe_2$, and Ni_3Se_4–$MoSe_2$ with different ratios were investigated in the 0.5 M H_2SO_4 solution in a three-electrode cell. For reference, commercial Pt/C (10 wt%) was also tested for comparison. As shown in Figure 5a, all Ni_3Se_4–$MoSe_2$ composites showed low onset overpotentials at a cathode current density of 1 mA/cm^2 (η_1). Specifically, Sample 1 showed the lowest onset overpotential of ~145 mV, while the overpotential for Samples 2 and 3 were ~160 and ~214 mV, respectively. Further, increasing the negative potential gave rise to a rapid increase in cathode current density. The overpotentials at the cathode current density of 10 mA/cm^2 (η_{10}), which are usually regarded as indicators of HER performance [49], were 206, 242, and 310 mV for Samples 1, 2, and 3, respectively. All of them showed a decrease in η_1 and η_{10} compared with pure $MoSe_2$ nanosheets. The Tafel plots of catalyst samples and Pt/C are displayed in Figure 5b. The linear regions of Tafel plots derived from the polarization curve can be analyzed using the Tafel equation:

η = b log j + a, where η is overpotential, b is Tafel slope, and j is current density [50,51]. Compared to pristine $MoSe_2$ nanosheets (Tafel slope of 80 mV/dec), Sample 1 showed the lowest Tafel slope (65 mV/dec), while a slightly higher Tafel slope value was observed for Sample 2 (76 mV/dec) and Sample 3 (96 mV/dec).The HER performance of pure Ni_3Se_4 nanoparticles was also investigated for comparison. They exhibited inferior performance towards HER. These results indicate that HER catalytic activity originates from $MoSe_2$ rather than from the inactive Ni_3Se_4. This observation is also confirmed by EIS, which was performed to investigate the impedance properties and the electron transfer kinetics during the HER [51]. The charge transfer resistance (R_{ct}) obtained from the impedance spectra (Figure 5c) showed that Ni_3Se_4 nanoparticles were conductive and had lower R_{ct} than pure $MoSe_2$ nanosheets, although they were not good for HER. We attribute the enhanced HER activity of $MoSe_2$ to the incorporation of Ni_3Se_4 nanoparticles, which have large surface areas and can improve the conductivity of $MoSe_2$ nanosheets and hence promote electron transfer between $MoSe_2$ and the electrolyte. The η_1, η_{10}, Tafel slope, and R_{ct} values of the three samples, along with those of Ni_3Se_4, $MoSe_2$ are summarized in Table 1.

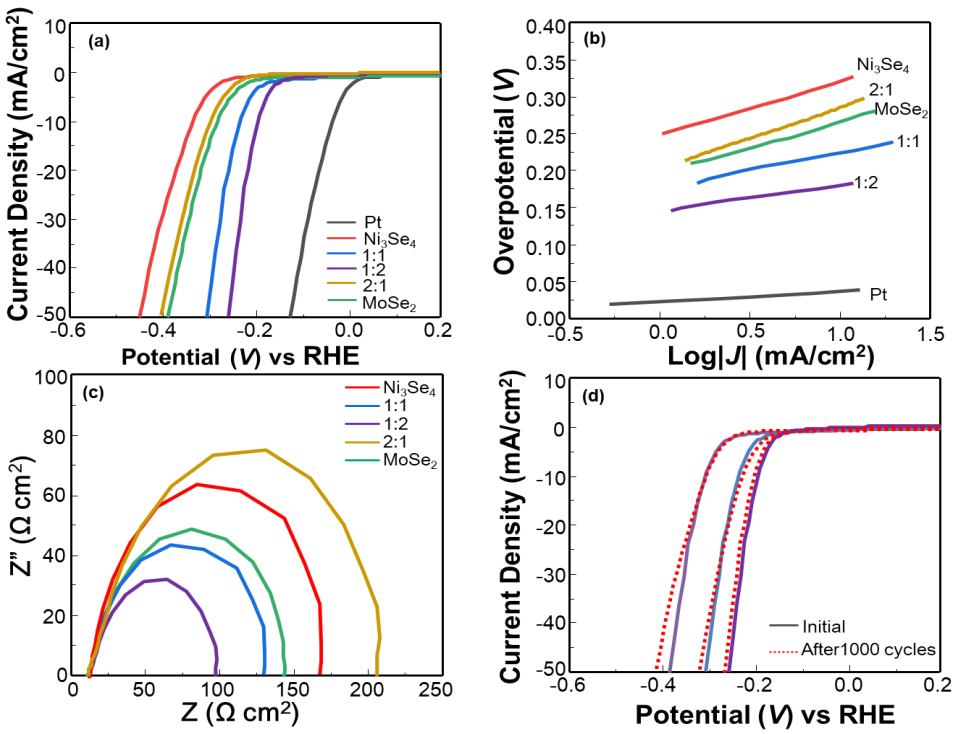

Figure 5. (**a**) Hydrogen evolution reaction (HER) polarization curves and (**b**) Tafel slopes of $MoSe_2$, Ni_3Se_4, Ni_3Se_4@$MoSe_2$, and Pt. (**c**) Impedance spectra of $MoSe_2$, Ni_3Se_4, and Ni_3Se_4@$MoSe_2$, and (**d**) stability of Ni_3Se_4@$MoSe_2$.

Table 1. Summary of η_1, η_{10}, Tafel slope, and R_{ct} of Ni_3Se_4, Ni_3Se_4–$MoSe_2$ composites, and $MoSe_2$.

	η_1 (mV)	η_{10} (mV)	Tafel Slope (mV/dec)	R_{ct} (Ω cm^2)
Ni_3Se_4	240	330	109	108
Ni_3Se_4–$MoSe_2$ (1:2)	145	206	65	68
Ni_3Se_4–$MoSe_2$ (1:1)	160	242	76	98
Ni_3Se_4–$MoSe_2$ (2:1)	214	310	96	156
$MoSe_2$	210	295	80	134

The stability of the Ni_3Se_4–$MoSe_2$ composites was evaluated by cyclic voltammetry tests from −0.4 to 0.2 V vs. RHE at 50 mV/s for 1000 cycles. The polarization curves of the Ni_3Se_4–$MoSe_2$ composites showed negligible activity change after 1000 cycles, indicating their durability towards HER. Notably,

the composites with ratios of 1:2 and 1:1 exhibited better stability than that with a ratio of 2:1, which is consistent with the HER performance results.

4. Conclusions

In summary, we successfully synthesized Ni_3Se_4–$MoSe_2$ composites by directly growing $MoSe_2$ on Ni_3Se_4 nanosheets for the first time. The Ni_3Se_4 nanosheets served as templates to support $MoSe_2$ and were expected to prevent $MoSe_2$ from aggregation and improve its conductivity. XRD, XPS, FE-SEM, and TEM were used to characterize the morphology and structure of the samples. The results revealed that $MoSe_2$ was chemically bonded on the surface of Ni_3Se_4. Further, electrochemical measurements of the composites verified that the HER performance was improved compared to pristine $MoSe_2$ nanosheets, whereas the Ni3Se4 nanosheets were not catalytically active to the HER but could reduce the charge transfer resistance and facilitate electron transfer between $MoSe_2$ and the electrolyte. The Ni_3Se_4–$MoSe_2$ composites with a ratio of 1:2 performed the best, with a small overpotential of 145 mV and a low Tafel slope of 65 mV/dec. Continued increase in the amount of Ni_3Se_4 led to inferior HER performance. These results suggest that the HER activity of $MoSe_2$ nanosheets can be enhanced by constructing composites with Ni_3Se_4 in appropriate ratios.

Supplementary Materials: The following are available online at http://www.mdpi.com/2076-3417/9/23/5035/s1: Figure S1: EDX spectra of Ni_3Se_4@$MoSe_2$; Figure S2: (a), (b), (c) SEM images of Ni_3Se_4@$MoSe_2$ with different Ni_3Se_4:$MoSe_2$ ratios of 1:2, 1:1, and 2:1, respectively.

Author Contributions: W.G. and Q.V.L. conceived and designed the experiments; W.G. performed the experiments; H.H.D., S.-R.B., A.H., M.T. and T.H.L. helped for data measuring and analysis; W.G. and Q.V.L. wrote the paper; Both the authors discussed the results and commented on the manuscript. S.Y.K., S.H.A. and H.W.J. are the corresponding author for the whole work.

Funding: This work was supported in part by the Basic Research Laboratory of the NRF funded by the Korean Government [grant number 2018R1A4A1022647] and in part by the Chung-Ang University Research Scholarship Grants in 2018.

Conflicts of Interest: The authors declare no conflicts of interest.

References

1. Dunn, S. Hydrogen futures: Toward a sustainable energy system. *Int. J. Hydrog. Energy* **2002**, *27*, 235–264. [CrossRef]
2. Momirlan, M.; Veziroglu, T. Current status of hydrogen energy. *Renew. Sustain. Energy Rev.* **2002**, *6*, 141–179. [CrossRef]
3. Dresselhaus, M.; Thomas, I. Alternative energy technologies. *Nature* **2001**, *414*, 332. [CrossRef] [PubMed]
4. Walter, M.G.; Warren, E.L.; McKone, J.R.; Boettcher, S.W.; Mi, Q.; Santori, E.A.; Lewis, N.S. Solar water splitting cells. *Chem. Rev.* **2010**, *110*, 6446–6473. [CrossRef]
5. Xie, J.; Zhang, H.; Li, S.; Wang, R.; Sun, X.; Zhou, M.; Zhou, J.; Lou, X.W.; Xie, Y. Defect-rich MoS_2 ultrathin nanosheets with additional active edge sites for enhanced electrocatalytic hydrogen evolution. *Adv. Mater.* **2013**, *25*, 5807–5813. [CrossRef] [PubMed]
6. Cortright, R.D.; Davda, R.; Dumesic, J.A. Hydrogen from catalytic reforming of biomass-derived hydrocarbons in liquid water. In *Materials For Sustainable Energy: A Collection of Peer-Reviewed Research and Review Articles from Nature Publishing Group*; World Scientific: Singapore, 2011; pp. 289–292.
7. Ball, M.; Wietschel, M. The future of hydrogen–opportunities and challenges. *Int. J. Hydrog. Energy* **2009**, *34*, 615–627. [CrossRef]
8. Deng, J.; Ren, P.; Deng, D.; Yu, L.; Yang, F.; Bao, X. Highly active and durable non-precious-metal catalysts encapsulated in carbon nanotubes for hydrogen evolution reaction. *Energy Environ. Sci.* **2014**, *7*, 1919–1923. [CrossRef]
9. Bard, A.J.; Fox, M.A. Artificial photosynthesis: Solar splitting of water to hydrogen and oxygen. *Chem. Res.* **1995**, *28*, 141–145. [CrossRef]
10. Turner, J.A. Sustainable hydrogen production. *Science* **2004**, *305*, 972–974. [CrossRef]

11. Li, Y.; Wang, H.; Xie, L.; Liang, Y.; Hong, G.; Dai, H. MoS_2 nanoparticles grown on graphene: An advanced catalyst for the hydrogen evolution reaction. *J. Am. Chem. Soc.* **2011**, *133*, 7296–7299. [CrossRef]
12. Conway, B.; Tilak, B. Interfacial processes involving electrocatalytic evolution and oxidation of H_2, and the role of chemisorbed H. *Electrochim. Acta* **2002**, *47*, 3571–3594. [CrossRef]
13. Kemppainen, E.; Bodin, A.; Sebok, B.; Pedersen, T.; Seger, B.; Mei, B.; Bae, D.; Vesborg, P.C.K.; Halme, J.; Hansen, O. Scalability and feasibility of photoelectrochemical H_2 evolution: The ultimate limit of Pt nanoparticle as an HER catalyst. *Energy Environ. Sci.* **2015**, *8*, 2991–2999. [CrossRef]
14. Elezović, N.R.; Gajić-Krstajić, L.; Radmilović, V.; Vračar, L.; Krstajić, N.V. Effect of chemisorbed carbon monoxide on Pt/C electrode on the mechanism of the hydrogen oxidation reaction. *Electrochim. Acta* **2009**, *54*, 1375–1382. [CrossRef]
15. Chen, C.; Kang, Y.; Huo, Z.; Zhu, Z.; Huang, W.; Xin, H.L.; Snyder, J.D.; Li, D.; Herron, J.A.; Mavrikakis, M. Highly crystalline multimetallic nanoframes with three-dimensional electrocatalytic surfaces. *Science* **2014**, *343*, 1339–1343. [CrossRef] [PubMed]
16. Ring, L.; Pollet, B.G.; Chatenet, M.; Abbou, S.; Küpper, K.; Schmidt, M.; Huck, M.; Gries, A.; Steinhart, M.; Schäfer, H. From bad electrochemical practices to an environmental and waste reducing approach for the generation of active hydrogen evolving electrodes. *Angew. Chem.* **2019**, *131*, 2–12. [CrossRef]
17. Zou, X.; Zhang, Y. Noble metal-free hydrogen evolution catalysts for water splitting. *Chem. Soc. Rev.* **2015**, *44*, 5148–5180. [CrossRef]
18. Liu, J.; Liu, Y.; Liu, N.; Han, Y.; Zhang, X.; Huang, H.; Lifshitz, Y.; Lee, S.-T.; Zhong, J.; Kang, Z. Metal-free efficient photocatalyst for stable visible water splitting via a two-electron pathway. *Science* **2015**, *347*, 970–974. [CrossRef]
19. Guo, S.; Zhang, S.; Wu, L.; Sun, S. Co/CoO nanoparticles assembled on graphene for electrochemical reduction of oxygen. *Angew. Chem.* **2012**, *124*, 11940–11943. [CrossRef]
20. Cao, R.; Lee, J.S.; Liu, M.; Cho, J. Recent progress in non-precious catalysts for metal-air batteries. *Adv. Energy Mater.* **2012**, *2*, 816–829. [CrossRef]
21. Wang, H.; Lu, Z.; Xu, S.; Kong, D.; Cha, J.J.; Zheng, G.; Hsu, P.-C.; Yan, K.; Bradshaw, D.; Prinz, F.B. Electrochemical tuning of vertically aligned MoS_2 nanofilms and its application in improving hydrogen evolution reaction. *Proc. Natl. Acad. Sci. USA* **2013**, *110*, 19701–19706. [CrossRef]
22. Tan, C.; Zhang, H. Two-dimensional transition metal dichalcogenide nanosheet-based composites. *Chem. Soc. Rev.* **2015**, *44*, 2713–2731. [CrossRef] [PubMed]
23. Chhowalla, M.; Shin, H.S.; Eda, G.; Li, L.-J.; Loh, K.P.; Zhang, H. The chemistry of two-dimensional layered transition metal dichalcogenide nanosheets. *Nat. Chem.* **2013**, *5*, 263. [CrossRef] [PubMed]
24. Nicolosi, V.; Chhowalla, M.; Kanatzidis, M.G.; Strano, M.S.; Coleman, J.N. Liquid exfoliation of layered materials. *Science* **2013**, *340*, 1226419. [CrossRef]
25. Kibsgaard, J.; Chen, Z.; Reinecke, B.N.; Jaramillo, T.F. Engineering the surface structure of MoS_2 to preferentially expose active edge sites for electrocatalysis. *Nat. Mater.* **2012**, *11*, 963. [CrossRef]
26. Choi, W.I.; Wood, B.C.; Schwegler, E.; Ogitsu, T. Site-dependent free energy barrier for proton reduction on MoS_2 edges. *J. Phys. Chem. C* **2013**, *117*, 21772–21777. [CrossRef]
27. Jaramillo, T.F.; Jørgensen, K.P.; Bonde, J.; Nielsen, J.H.; Horch, S.; Chorkendorff, I. Identification of active edge sites for electrochemical H_2 evolution from MoS_2 nanocatalysts. *Science* **2007**, *317*, 100–102. [CrossRef]
28. Lauritsen, J.; Nyberg, M.; Nørskov, J.K.; Clausen, B.; Topsøe, H.; Lægsgaard, E.; Besenbacher, F. Hydrodesulfurization reaction pathways on MoS_2 nanoclusters revealed by scanning tunneling microscopy. *J. Catal.* **2004**, *224*, 94–106. [CrossRef]
29. Guo, W.; Le, Q.; Hasani, A.; Lee, T.; Jang, H.; Luo, Z.; Kim, S. MoSe2-GO/rGO Composite Catalyst for Hydrogen Evolution Reaction. *Polymers* **2018**, *10*, 1309. [CrossRef]
30. Tang, H.; Dou, K.; Kaun, C.-C.; Kuang, Q.; Yang, S. $MoSe_2$ nanosheets and their graphene hybrids: Synthesis, characterization and hydrogen evolution reaction studies. *J. Mater. Chem.* **2014**, *2*, 360–364. [CrossRef]
31. Qu, B.; Li, C.; Zhu, C.; Wang, S.; Zhang, X.; Chen, Y. Growth of $MoSe_2$ nanosheets with small size and expanded spaces of (002) plane on the surfaces of porous N-doped carbon nanotubes for hydrogen production. *Nanoscale* **2016**, *8*, 16886–16893. [CrossRef]
32. Gao, M.-R.; Lin, Z.-Y.; Zhuang, T.-T.; Jiang, J.; Xu, Y.-F.; Zheng, Y.-R.; Yu, S.-H. Mixed-solution synthesis of sea urchin-like NiSe nanofiber assemblies as economical Pt-free catalysts for electrochemical H_2 production. *J. Mater. Chem.* **2012**, *22*, 13662–13668. [CrossRef]

33. Tang, C.; Cheng, N.; Pu, Z.; Xing, W.; Sun, X. NiSe nanowire film supported on nickel foam: An efficient and stable 3D bifunctional electrode for full water splitting. *Angew. Chem. Int. Ed.* **2015**, *54*, 9351–9355. [CrossRef] [PubMed]
34. Ji, L.; Lv, C.; Chen, Z.; Huang, Z.; Zhang, C. Nickel-Based (Photo) Electrocatalysts for Hydrogen Production. *Adv. Mater.* **2018**, *30*, 1705653. [CrossRef] [PubMed]
35. Zhang, T.; Liu, X.; Cui, X.; Chen, M.; Liu, S.; Geng, B. Colloidal Synthesis of Mo–Ni Alloy Nanoparticles as Bifunctional Electrocatalysts for Efficient Overall Water Splitting. *Adv. Mater. Interfaces* **2018**, *5*, 1800359. [CrossRef]
36. Tian, J.; Cheng, N.; Liu, Q.; Sun, X.; He, Y.; Asiri, A.M. Self-supported NiMo hollow nanorod array: An efficient 3D bifunctional catalytic electrode for overall water splitting. *J. Mater. Chem. A* **2015**, *3*, 20056–20059. [CrossRef]
37. Zhou, X.; Liu, Y.; Ju, H.; Pan, B.; Zhu, J.; Ding, T.; Wang, C.; Yang, Q. Design and epitaxial growth of $MoSe_2$–NiSe vertical heteronanostructures with electronic modulation for enhanced hydrogen evolution reaction. *Chem. Mater.* **2016**, *28*, 1838–1846. [CrossRef]
38. Merki, D.; Vrubel, H.; Rovelli, L.; Fierro, S.; Hu, X. Fe, Co, and Ni ions promote the catalytic activity of amorphous molybdenum sulfide films for hydrogen evolution. *Chem. Sci.* **2012**, *3*, 2515–2525. [CrossRef]
39. Kuraganti, V.; Jain, A.; Bar-Ziv, R.; Ramasubramaniam, A.; Bar-Sadan, M. Manganese doping of $MoSe_2$ promotes active defect sites for hydrogen evolution. *ACS Appl. Mater. Interfaces* **2019**, *11*, 25155–25162. [CrossRef]
40. Peng, H.; Zhou, J.; Sun, K.; Ma, G.; Zhang, Z.; Feng, E.; Lei, Z. High-performance asymmetric supercapacitor designed with a novel NiSe@ $MoSe_2$ nanosheet array and nitrogen-doped carbon nanosheet. *ACS Sustain. Chem. Eng.* **2017**, *5*, 5951–5963. [CrossRef]
41. Chen, H.; Wu, L.; Zhang, K.; Qin, A.; Chen, S. New Synthesis of Polycrystalline NiSe Nanoarrays on Ni Foam as the Electrode for High Performance Supercapacitors. *Int. J. Electrochem. Sci.* **2018**, *13*, 12437–12449. [CrossRef]
42. Lee, C.-T.; Peng, J.-D.; Li, C.-T.; Tsai, Y.-L.; Vittal, R.; Ho, K.-C. Ni_3Se_4 hollow architectures as catalytic materials for the counter electrodes of dye-sensitized solar cells. *Nano Energy* **2014**, *10*, 201–211. [CrossRef]
43. Zhang, J.-Y.; Tian, X.; He, T.; Zaman, S.; Miao, M.; Yan, Y.; Qi, K.; Dong, Z.; Liu, H.; Xia, B.Y. In situ formation of Ni_3Se_4 nanorod arrays as versatile electrocatalysts for electrochemical oxidation reactions in hybrid water electrolysis. *J. Mater. Chem. A* **2018**, *6*, 15653–15658. [CrossRef]
44. Anantharaj, S.; Kennedy, J.; Kundu, S. Microwave-initiated facile formation of Ni_3Se_4 nanoassemblies for enhanced and stable water splitting in neutral and alkaline media. *ACS Appl. Mater. Interfaces* **2017**, *9*, 8714–8728. [CrossRef] [PubMed]
45. Bhat, K.S.; Nagaraja, H. Nickel selenide nanostructures as an electrocatalyst for hydrogen evolution reaction. *Int. J. Hydrog. Energy* **2018**, *43*, 19851–19863. [CrossRef]
46. Anantharaj, S.; Karthik, K.; Amarnath, T.S.; Chatterjee, S.; Subhashini, E.; Swaathini, K.C.; Karthick, P.E.; Kundu, S. Membrane free water electrolysis under 1.23 V with Ni_3Se_4/Ni anode in alkali and Pt cathode in acid. *Appl. Surf. Sci.* **2019**, *478*, 784–792. [CrossRef]
47. Peng, H.; Wei, C.; Wang, K.; Meng, T.; Ma, G.; Lei, Z.; Gong, X. $Ni_{0.85}Se$@ $MoSe_2$ nanosheet arrays as the electrode for high-performance supercapacitors. *ACS Appl. Mater. Interfaces* **2017**, *9*, 17067–17075. [CrossRef]
48. Du, J.; Zou, Z.; Liu, C.; Xu, C. Hierarchical Fe-doped Ni_3Se_4 ultrathin nanosheets as an efficient electrocatalyst for oxygen evolution reaction. *Nanoscale* **2018**, *10*, 5163–5170. [CrossRef]
49. Zhang, L.; Sun, L.; Huang, Y.; Sun, Y.; Hu, T.; Xu, K.; Ma, F. Hydrothermal synthesis of N-doped RGO/$MoSe_2$ composites and enhanced electro-catalytic hydrogen evolution. *J. Mater. Sci.* **2017**, *52*, 13561–13571. [CrossRef]
50. Xu, C.; Peng, S.; Tan, C.; Ang, H.; Tan, H.; Zhang, H.; Yan, Q. Ultrathin S-doped $MoSe_2$ nanosheets for efficient hydrogen evolution. *J. Mater. Chem. A* **2014**, *2*, 5597–5601. [CrossRef]
51. Voiry, D.; Yang, J.; Chhowalla, M. Recent strategies for improving the catalytic activity of 2D TMD nanosheets toward the hydrogen evolution reaction. *Adv. Mater.* **2016**, *28*, 6197–6206. [CrossRef]